Seventeen-GHz Directional Coupler Optical Modulator

Mark Yu and Anand Gopinath

Abstract—**The design of our high-speed directional coupler modulators at 0.83 μm used a semi-vectorial finite difference solver to obtain the odd and even mode optical propagation constants in the AlGaAs waveguide structure and a quasistatic finite difference code to obtain the RF characteristics of the electrode structure, which was an asymmetric coplanar waveguide modified capacitance loading. The measured drive voltage of the modulators, for 10–90% response, varied between 22 and 27 V, compared with the theoretical value of 25 V. The 3 dB bandwidth of 17 GHz was obtained for this capacitive-loaded design, with 2500 mm interaction length, and is in good agreement with the predicted result.**

I. Introduction

IN THIS paper we discuss the design and realization of a 17 GHz directional coupler modulator/switch at 830 nm wavelength. High bit rate systems require that the signals modulate the optical carrier, and the most efficient form is direct laser modulaton, but this suffers from spectral broadening. A monochromatic carrier is generally used for long distance transmission in optical fibers, necessitating the development of external modulators. Two types of electrooptic modulators are commonly used, and these are the linear electrooptic modulators employing the linear electrooptic effect (Pockels effect) and the electroabsorption modulators based on the Franz-Keldysh or the Quantum Confined Stark effect. In this study we have confined our design to the linear electrooptic devices.

Electrooptic modulators are either the interferometric type or the directional coupler type. The directional coupler switch/modulator is the focus of this study because it may be used as a 2×2 switch as well as a modulator. The bandwidth of the traveling-wave electrooptic modulator is usually determined by the difference in velocity of the optical and electrical signals. In our design, we have used a capacitively loaded coplanar guide structure to equalize the optical and rf indices. A large value of the overlap integral and good velocity matching are required for low power drive and high speed. Good dc response and low power requirements may be obtained with asymmetric excitation of electrodes, but the RF loss becomes high [1]. To lower the RF loss, we must use wide RF electrodes with asymmetric excitation. Since the bandwidth also depends on the RF impedance matching and loss, as well as the optical-electrical phase velocity mismatch, some of the tradeoff relations are discussed in the design of our modulator. In the following sections, we discuss the simulation issues, the design options, and, finally, our measured results.

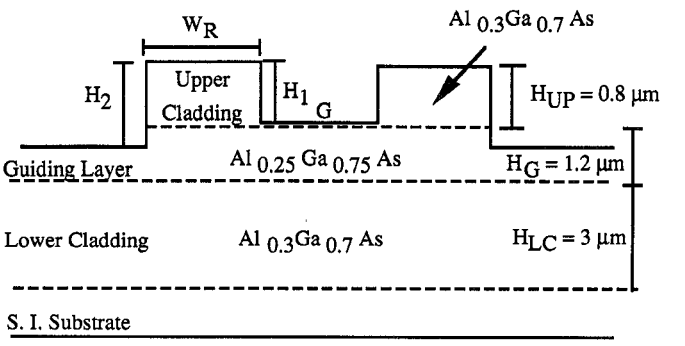

Fig. 1. Cross-section of the double heterostructure AlGaAs/GaAs directional coupler modulator used in this project.

II. Simulation of Directional Coupler Modulator

A. Optical Waveguide Calculations

To calculate the modal behavior of the optical guides, a computer program developed by Klein Johnson, University of Minnesota [2], was used that utilizes the nonuniform mesh implementation of the semi-vectorial finite difference method [3] for determining polarized **E** field solution of the Helmholtz equation in rib waveguides with arbitrary refractive index profiles. The cross-section of the AlGaAs/GaAs structure used in our directional coupler is shown in Fig. 1, and we used above method for determining the TE mode structure at 0.83 μm wavelength. The field distributions in this layer structure are obtained for various waveguide ridge widths W_r, ridge heights H_2, and differential depth $H_1 - H_2$ to determine the guide dimensions, so that only one odd and one even mode propagate. In order to establish large optical coupling between waveguides, the gap G between the guides, shown in Fig. 1, was chosen to be 2 μm, and the ridge width of the waveguides was chosen to be 3 μm. H_2 was set at 0.95 μm, and this ensures that the propagation of only one odd and one even mode occurs.

B. Electrode Calculations

For the directional coupler devices discussed here, the asymmetric coplanar strip was used. Losses in these transmission lines have been investigated by several authors [4]–[9].

Manuscript received January 10, 1995; revised May 1, 1995. This work was supported in part by NSF and by ARPA, under a contract with US Air Force Rome Laboratories.

The authors are with the Department of Electrical Engineering, University of Minnesota, Minneapolis, MN 55455 USA.

IEEE Log Number 9413706.

We have written a simulation program using the quasistatic approach with a finite difference nonuniform mesh method to calculate the conductor loss and the strip impedance on AlGaAs/GaAs substrates. With this program, we are able to determine the electric field distributions, electrode impedance, and losses for any RF strip waveguide geometry. The structure analyzed for this project is the nonplanar asymmetric coplanar waveguide with thick electrodes. The program obtains the potential and electric field distribution using the same nonuniform mesh implementation as that used in the semivectorial finite difference program for the optical modes, so that the overlap integral between the optical and electric fields may be obtained directly. From the potential distribution, the capacitance between the rf electrode and the ground plane or planes may be obtained, with and without dielectric present, given as C_d and C_0, respectively. The microwave phase velocity factor is then given by $v_{\rm rf}/c_0 = \sqrt{C_0/C_d} = 1/n_{\rm rf}$ where c_0 is the velocity of light in air. The characteristic impedance is given by $Z_0 = 1/c_0\sqrt{C_0 C_d}$. The charge pattern without the dielectric substrate corresponds to the longitudinal current distribution pattern, and from this the conductor loss factor α_c is evaluated from [8]

$$\alpha_c = \frac{R_s}{2Z_0 I^2}\left[\int J_s^2 dl + \int J_{\rm gp}^2 dl\right] \tag{1}$$

where J_s is the strip longitudinal current linear density, $J_{\rm gp}$ is the ground-plane current linear density, I is the current carried by strip or ground-plane, and R_s is the metal surface resistivity in ohms. It is assumed that the current is confined to the surface of the electrode which is valid at frequencies at which the skin depth is less than half the electrode thickness t. At low frequencies, when the skin depth is large compared to the electrode thickness t, the sheet resistance and loss are expected to become independent of frequency, and a reasonable approximation for R_s at low frequency is $R_s = 2/\sigma t$, where σ is the conductivity of the electrode metal. As indicated earlier, comparisons with other published work for planar electrode structures on $LiNBO_3$ and GaAs show excellent agreement [8], [10].

C. Response of Directional Coupler Modulator

The frequency response of a directional coupler traveling wave optical modulator depends on the detailed phase velocity difference ($\Delta\beta$) between the two optical guides along the device length, rather than the integrated value of $\Delta\beta$ of the coupler [11]. The response of a directional coupler modulator to a step voltage is therefore determined by dividing the coupler into small segments and using the Fast Fourier Transform to calculate the Fourier coefficients of the voltage in each section. Since the electrical loss on the transmission line is frequency dependent, the transfer matrix function of each section is then obtained by using Fourier series analysis together with the conductor loss factor, and the overall transfer function is obtained by matrix multiplication [10]. In the present case, we are only interested in the frequency response of the coupler, and therefore the calculation is performed by segmenting the coupler, with single frequency of excitation. A sketch of the directional coupler modulator is shown in Fig. 2

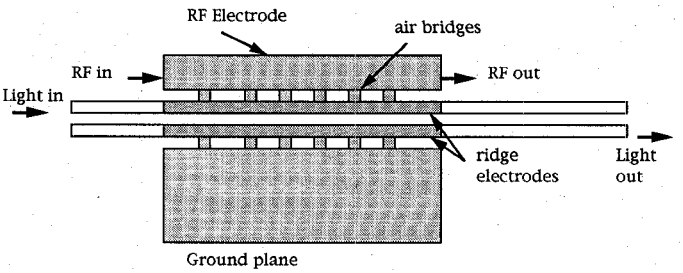

Fig. 2. The optical modulator schematic with capacitive-loaded electrode structure.

and the analysis on the segmented coupler is performed by the usual coupled mode matrix calculation for each segment. The coherent optical signals in the two waveguides are represented by the complex amplitudes $r(z)$ and $s(z)$, which vary slowly in the propagation direction of z-axis. Application of a voltage $v(t)$ to the electrode induces a mismatch $\Delta\beta(V) = \beta_2 - \beta_1$ between two propagation constants of guides 1 and 2. The energy exchange between two guides is governed by the coupled-mode equations [13], given by

$$\frac{dr}{dz} = j\delta r - j\kappa s \tag{2}$$

$$\frac{ds}{dz} = -j\delta s - j\kappa r \tag{3}$$

where $\delta = \Delta\beta/2$, and κ is the coupling coefficient. For any input amplitudes r_0 and s_0, the coupled mode equations may be written in matrix form

$$\begin{pmatrix} r \\ s \end{pmatrix} = h \begin{pmatrix} r_0 \\ s_0 \end{pmatrix} \tag{4}$$

where

$$h = \begin{pmatrix} A & -jB \\ -jB^* & A^* \end{pmatrix}. \tag{5}$$

Note that the asterisk indicates the complex conjugate. The matrix elements are given as

$$A = \cos\psi + j\frac{\delta z}{\psi}\sin\psi \tag{6}$$

$$b = \frac{\kappa z}{\psi}\sin\psi \tag{7}$$

where $\psi = \sqrt{(\kappa z)^2 + (\delta z)^2}$. The required drive voltage is independent of the electrode type, but the expected modulation bandwidth for the traveling-wave electrode is quite different from the lumped electrode case. To examine the bandwidth limitation of the directional coupler modulator taking into account of microwave loss, we assume that the driving signal over the length Δl for the time interval Δt is given by

$$V(\delta l, \Delta t) = V_{\rm dc} + V_0 \sin\left[\omega_{\rm rf}\Delta t - \frac{2\pi f_{\rm rf}}{c_0}(n_{\rm op} - n_{\rm rf})\Delta l\right] e^{\alpha(f_{rf})z} \tag{8}$$

where $V_{\rm dc}$ is the dc voltage, $n_{\rm rf}$ is the RF index, $n_{\rm op}$ is the effective optical mode index, and $f_{\rm rf}$ is the RF discrete frequency. $(n_{\rm op} - n_{\rm rf})$ is a measure of the velocity mismatch between the optical and microwave signals, and for $n_{\rm op} = n_{\rm rf}$

the optical wave travels down the waveguide at the same speed as the microwave drive signal. The effective electrooptical induced index change within a cross-section of the optical mode may be written as

$$\Delta n(V) = -\frac{n^3 r}{2}\frac{V}{G}\Gamma \tag{9}$$

where G is the interelectrode gap and, $n^3 r$ is 49×10^{-6} μm/V for GaAs/AlGaAs [12], and Γ is the overlap integral between the applied DC field $\mathbf{E}$ and the optical field distribution $\mathbf{E}_{\text{op}}$. Thus

$$\Gamma = \frac{G}{V}\int\int_S \mathbf{E}|\mathbf{E}_{\text{op}}|^2 dS. \tag{10}$$

The efficiency of dc response of an optical modulator is determined by the overlap integral. The total phase shift induced by the electrooptical index change over a small interaction length Δl is then given by [12] is given by

$$\Delta\beta\Delta l = \frac{-\pi n^3 r}{2}\Gamma\frac{V(\Delta l, \Delta t)}{G}\frac{\Delta l}{\lambda}. \tag{11}$$

Substituting for $\delta = \Delta\beta/2$, and the other terms from above into (7), we obtain the transfer function h as a function of time and distance in the propagation direction for a discrete frequency.

III. Modulator Design

The waveguide layers for the design of our waveguide device are shown in Fig. 1, consists of a 1.2-μm-thick $Al_{0.25}Ga_{0.75}As$ guiding layer sandwiched by $Al_{0.3}Ga_{0.7}As$ upper and lower cladding layers for 0.8 and 3 μm, respectively. The Al mole fractions in these layers were selected for low bandedge absorption in the guiding layer and low defects in cladding layers. The relationship between the switching voltage-coupling length product V_cL_c and the differential etching depth $(H_2 - H_1)$ is complex. The total phase shift $\Delta\beta L_c$ over the interaction length is a function of overlap integral Γ and V_cL_c. Since the goal in modulator design is high modulation bandwidth with low drive voltage, for the given material GaAs/AlGaAs and wavelength 830 nm we minimize V_cL_c by optimizing the Γ for a constant electrode gap. Using the design algorithms for optical and electric fields, calculated results for V_c with 97% power transfer between guides, Γ, L_c, and coupling coefficient κ with respect to several differential depths are summarized in Table I. In order to obtain efficient overlap integral, the electrodes were placed on top of and by the side of the ridge waveguides. It is obvious from Table I that the center etching depth has little effect on the voltage-length product when the gap between guides is kept constant. It also indicates that for the design of modulators, a large value of coupling coefficient is simply not sufficient for a good overlap integral. A differential-etch design of the coupler was chosen, where the etch depth of the center gap is 0.2 μm shallower than the outer edge due to the small V_cL_c. This feature provides stronger coupling between guides, which results in a short coupling length, but the voltage requirement will be higher. As shown in Table I, the voltage increases from 8 to 25 V as the coupling length reduces from 9308 to 2504 μm. To keep the device length small, we have chosen this value of differential etch depth, despite this large switching voltage, for the results in this paper.

TABLE I
Simulation Results of Voltage-Length Product for Several Differential Depths, with 2 μm Gap Between Optical Guides, 3 μm Ridge Width, and $H_2 = 0.95$ μm

H_2-H_1 (μm)	V_c (V)	L_c (μm)	κ (/cm)	Γ	V_cL_c (V-cm)
0 0	8	9308	1 7	0 586	7.45
*0.2	25	2515	5.7	0.591	6.76
0.3	67	1017	15.4	0.605	6.81
0.5	124	551	28.5	0.598	6.83

* The differential depth used in this work.

A. Electrode Design

It is well known that efficiency and bandwidth of traveling-wave waveguide optical modulators are limited by the mismatch of the optical and the electrical phase velocities, which results in an increase of the RF drive level requirement for adequate modulation. Most broad-band modulators reported to date [14]–[17] still require high drive power. For the coupler an additional constraint is the coupling length of the device. To overcome the problem of velocity mismatch, several velocity-matching techniques have been proposed for the optical modulators [18]–[20]. Only the electrical phase velocity may be adjusted for velocity-matching, and in III-V semiconductor structures this is larger than the optical phase velocity. The effective dielectric constant ϵ_{reff} of a coplanar transmission line is approximately given as $\epsilon_{\text{reff}} = (\epsilon_r + 1)/2 = 7$, with $\epsilon_r = 13$ for GaAs/AlGaAs, and the effective microwave refractive index n_{rf} becomes $\sqrt{\epsilon_{\text{reff}}} = 2.65$, so that the electrical phase velocity is 3.59/2.65 times higher in AlGaAs/GaAs waveguide. An electrode structure based on periodic capacitive-loading was designed, as shown in Fig. 2, where the RF signal line and ground plane are placed on either side of the optical waveguides and connected to electrodes on top of the ridges through several air bridges. As the RF signal is applied to one end of the electrode, it travels through the side electrode that has the capacitance C_d per unit length, and because of the air bridges to the electrode on top of the ridge, additional lumped capacitance C_d' will be added to the structure, as shown in Fig. 3. Thus, the effective microwave index for the capacitive-coupled electrode becomes $n_{\text{rf}}' = \sqrt{(C_d + C_d')/C_0}$, and the corresponding phase velocity becomes $v_{\text{rf}} = c_0/n_{\text{rf}}'$. We have modeled this electrode structure as a RF transmission line shunted by a succession of parallel lumped capacitances, resulting in an artificial transmission line, with a cutoff frequency. Several electrode structures with capacitive-loading for a coupling length of 2500 μm were analyzed, based on different values of S and W for the gap $G = 2$ μm. The value of n_{rf}'varied from 2.76–2.93, and the impedance varied from 33–39 ohms. Thus, with the capacitve-loading design, we can improve the velocity match substantially, but with a reduction of the cutoff of the RF bandwidth due to the artificial transmission line

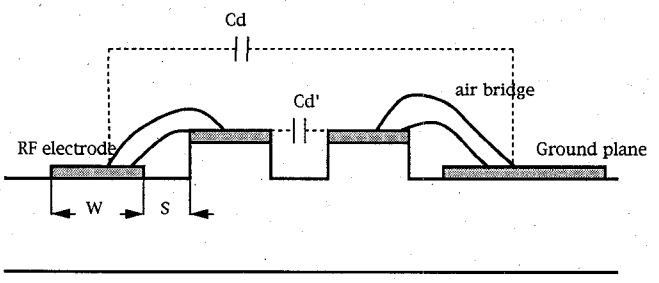

Fig. 3. The optical modulator cross-section with capacitive-loaded electrode structure showing the capacitances.

effect. We have simulated the small-signal relative response of the case with $W = 6$ mm and $S = 20$ mm, biased in the linear region of the transfer function for several different frequency-dependent losses, neglecting the artificial line cutoff effect. The results predict that for the RF line loss of 2 dB/cm, the half power bandwidth, is about 23 GHz an, for 4 dB/cm, the 3 dB bandwidth is about 20 GHz.

IV. Experimental Results

Several coupler modulators were built in AlGaAs/GaAs material system based on the above design considerations, using reactive ion etching to define the guides and Schottky barrier metallization with air bridges for the electrodes. We discuss the measurements and results in the following sections.

A. RF Electrode Measurements

The HP8510A NetworkAnalyzer was used to measure the RF characteristics of the electrodes using RF probes, and all measurements were made at a nominal input power of 10 dBm. The insertion loss and the impedance match for different separations of side electrode S, as well as its width W and electrode gap G, were obtained through the measurements of S_{21} and S_{11}, respectively. In our case, the ridge width was kept constant at 3 μm, G the gap between the electrodes on the ridge was kept constant at 2 μm, the spacing S between the RF electrode and the ridge was kept constant at 20 μm, the RF electrode width W was varied from 6 μm to 20 μm, and all electrodes had the same coupling length of 2500 μm. The results showed that the wider the RF electrode, the lower the insertion loss and the better the impedance match when the separation of side electrode from ridge is kept constant. For $W = 20$ μm, $S = 6$ μm, the 3 dB bandwidth is close to 16 GHz. From phase measurements of the S_{21}, we estimate the RF phase velocity and the slowing factor, but only consider the section of interaction, which is 2500 μm long. For the case of $W = 20$ μm, the measured phase delay leads to an effective RF index of 3.11.

B. Optical DC and High-Frequency Response

The experimental results of switching voltage listed in Table II are in good agreement with the theoretical values, with less than 7% difference. The measured switching voltages are slightly higher than the estimated value of 20 V mainly due to the low overlap integral of optical mode and applied electric field of about 60%, for an extinction ratio of approximately 94%.

TABLE II
Comparison of Experimental Results of Switching Voltage with Simulation Predictions for Capacitive-Loaded Modulators for Two Parameters

Interaction Length (μm)	W (μm)	S (μm)	Overlap Integral	Extinction Ratio (dB)	Switching Voltage (V) (measured)	Switching Voltage (V) (theory)
2500 (1 coupling)	6	20	59.1%	12.4 (94.5%)	27	25 (94%)
2500 (1 coupling)	20	20	60.2%	12.2 (94.3%)	22	24 (94%)

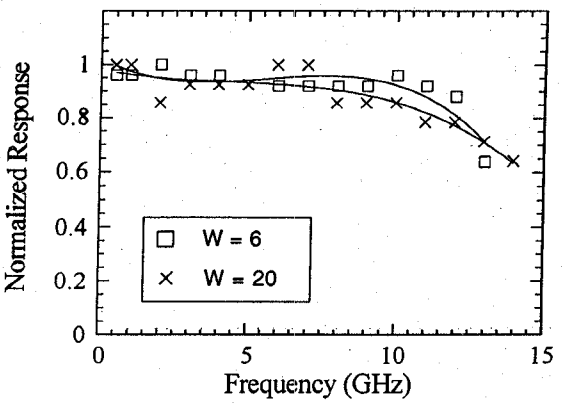

Fig. 4. High speed response of capacitively loaded modulator with $S = 20$ μm for $W = 6$ μm and 20 μm at 10 dBm RF power.

The high frequency optical characteristics of the optical modulator was measured by detection by high speed photo diode, through the use of lock-in amplifier synchronized to a reference pulsed signal in the input beam. The light signal is obtained from a 0.83 μm wavelength laser, which was pulsed at a 50% duty cycle for 0.5 ms pulses at 1 kHz repetition. The pulse signal was also sent to the reference port of the lock-in amplifier for synchronization with the demodulated signal. The laser light is coupled into the modulator, and a microwave signal from the HP8340A sweeper at a nominal power level of 10 dBm is applied to the modulator electrodes. DC voltage is biased at the midpoint of linear region where the optical output intensity is a linear function of the applied voltage. The modulation depth at 10 dBm power was about 4%. The modulated light was detected by a high speed photodiode, and the signal was fed into a microwave spectrum analyzer HP8593A. The output of the analyzer at its lowest IF then went to a detector diode and a RC circuit. The output signal from the envelope detection scheme was then connected to the signal port of the lock-in amplifier. Since the signal was synchronized with the reference pulse signal, the detection may be observed from the output dc level of the lock-in amplifier detector. The resulting amplitude modulation versus frequency are plotted for our modulators and given in Table II and plotted in Fig. 4. The measured bandwidth of the modulator with 2500 μm. interaction length for RF electrode widths of $W = 6$ and 20 μm, by extrapolation, are approximately 15 and 17 GHz, respectively, as shown in Fig. 4. The frequency response of the modulator is limited by the 3 dB bandwidth of the electrode design as a result of the capacitance loading.

V. SUMMARY

In this paper we have presented comprehensive simulation models of optical and electrical properties and the design of the high-speed directional coupler intensity electrooptic modulators at 0.83 μm. In the design of electrodes, the RF phase velocity is reduced by the capacitance loading, resulting in the increase of the microwave effective index. The effective index is more sensitive to the separation of RF source line from the ridge than the width of the RF line. The loaded capacitance is very efficient for the reduction of microwave phase velocity, however with a decrease of the RF bandwidth. The calculated small-signal response predicts that for a 40% improvement of phase velocity match, 17 GHz at 3 dB bandwidth can be achieved for RF loss factor less than 5 dB/cm. The dc switching voltages have been measured, and they vary between 22 and 27 V, which is less than 8% difference from the theoretical result of 25 V. The high speed response of the devices have also been measured and a 3 dB bandwidth at 17 GHz has been achieved. This is in good agreement with the 22 GHz theoretical value for microwave effective index at 3.1.

REFERENCES

[1] M. N. Khan, "Electrooptic waveguide directional coupler modulator in AlGaAs/GaAs," Ph.D. Thesis, 1992.

[2] K. L. Johnson and A. Gopinath, "Non-uniform implementation of the semivectorial finite difference method for dielectric waveguide structure," to be published in *J. Lightwave Technol.*

[3] M. S. Stern, "Semivectorial polarized finite difference method of optical waveguides with arbitrary index profiles," *IEE Proc.*, vol. 135, no. 1, pp. 56–63, 1988.

[4] B. E. Spielman, "Computer-aided analysis of dissipation losses in isolated and coupled transmission lines for microwave and millimeter-wave integrated circuit applications," Naval Research Laboratory Rep. 8009, Washington, DC, 1979.

[5] J. B. Davies and D. Mirshekar-Syakhal, "Spectral domain solution of arbitrary coplanar transmission line with multilayer substrates," *IEEE Trans. Microwave Theory Tech.*, vol. MTT-25, pp. 143–146, 1977.

[6] K. C. Gupta, R. Garg, and I. J. Bahl, *Microstrip Lines and Slot Lines*. Dedham, MA: Artech House, 1979.

[7] K. Kitazawa and T. Itoh, "Propagation characteristics of coplanar-type transmission lines with lossy media," *IEEE Trans. Microwave Theory Tech.*, vol. 39, pp. 1694–1700, 1991.

[8] A. Gopinath, "Losses in coplanar waveguides," *IEEE Trans. Microwave Theory Tech.*, vol. MTT-30, pp. 1101–1104, 1982.

[9] K. Koshiji and E. Shu, "Effect of inner conductor offset in a coplanar waveguide," *IEEE Trans. Microwave Theory Tech.*, vol. MTT-32, pp. 1387–1391, 1984.

[10] J. P. Donnelly and A. Gopinath, "A comparison of power requirements of traveling-wave $LiNbO_3$ optical couplers and interferometric modulators," *IEEE J. Quantum Electron.*, vol. QE-23, pp. 30–41, 1987.

[11] S. K. Koroky and R. C. Alferness, "Time and frequency-domain response of directional-coupler traveling-wave optical modulators," *J. Lightwave Technol.*, vol. 1, pp. 244–251, 1983.

[12] R. C. Alferness, "Waveguide electrooptic modulators," *IEEE Trans. Microwave Theory Tech.*, vol. MTT-30, pp. 1121–1137, 1982.

[13] A. Yariv, "Coupled mode theory for guided wave optics," *IEEE J. Quantum Electron.*, vol. QE-9, pp. 919–933, 1973.

[14] R. C. Alferness, S. K. Korotky, and E. A. J. Marcatili, "Velocity-matching techniques for integrated optictraveling wave switch/modulators," *IEEE J. Quantun Electron.*, vol. QE-20, pp. 301–309, 1984.

[15] T. Yoneyama, K. Niinuma, and S. Kanno, "Velocity-Matched $LiNbO_3$ waveguide optical modulator using inverted slot line," *IEEE Microwave and Guided Wave Lett.*, vol. 1, no. 8, pp. 192–194, 1990.

[16] W. B. Bridges, F. T. Sheehy, and J. H. Schaffner, "Velocity-matched electro-optic modulator," *SPIE*, San Jose, CA, vol. 1371, pp. 68–77, Sept. 17–18, 1990.

[17] S. Y. Wang, M. R. T. Tan, and Y. M. Houng, "Velocity-matched III-V traveling wave electro-optic modulator," *SPIE*, San Jose, CA, vol. 1371, pp. 98–103, Sept. 17–18, 1990.

[18] H. C. Hoyt, D. D. Simmonds, and W F. Rich, "Computer designed 805 MHz proton linac cavities," *Rev. Sci. Inst.*, vol. 37, no. 6, pp. 755–762, 1966.

[19] L. M. Field, "Some slow-wave structures for traveling-wave tubes," *Proc. IRE*, vol. 37, pp. 34–40, Jan. 1949.

[20] R. C. Fletcher, "Abroad-band interdigital circuit for use in traveling-wave-type amplifiers," *Proc. IRE*, vol. 40, pp. 951–958, Aug. 1952.

Mark Yu, photograph and biography not available at the time of publication.

Anand Gopinath, photograph and biography not available at the time of publication.